Supporting information

Regular Hexagonal CuBi Nanosheets Boost Highly Efficient CO_2 Reduction to HCOOH in Solid-Electrolyte Cell

Xiaoshan Wang[a], Xiang Fei[a], Mingwang Wang[a], Wenhang Wang[a], Zhongxue Yang[a], Hui Ning[a,*], Yunlong Zhang[a], Li Wang[b], Xin Jin[a] and Mingbo Wu[a,*]

[a]*State Key Laboratory of Heavy Oil Processing, College of Chemical Engineering, College of New Energy, Institute of New Energy, China University of Petroleum (East China), Qingdao, 266580*

[b]*Shandong Dongyue future hydrogen energy material Co., Ltd, Zibo City, 256412*

**Corresponding author. E-mail: wumb@upc.edu.cn (M.B. Wu); ninghui@upc.edu.cn (H. Ning)*

Calculation of faradaic efficiency

The faradaic efficiency of products was calculated as follows:

$$FE_{H_2\ or\ CO}\ (\%) = \frac{i_{H_2\ or\ CO}}{i_{Total}} \times\ 100\% = \frac{c_{H_2\ or\ CO} \times \nu \times \frac{2P_0F}{RT}}{i_{Total}} \times 100\%$$

i (A) is partial current of the H_2 and CO product.

c (ppm) is the volume concentrations of H_2 and CO analyzed by GC.

ν (ml min^{-1}) is gas flow rate.

P_0 is the atmosphere pressure (1.013 bar).

T is the temperature (298 K).

R is the ideal gas constant (83.14 mL bar mol^{-1} K^{-1}).

$$FE_{HCOOH}\ (\%) = \frac{Q_{HCOOH}}{Q_{Total}} \times\ 100\% = \frac{C_{HCOOH} \times V \times N \times F}{Q_{Total}} \times 100\%$$

C (mol L^{-1}) is concentration of formate in the electrolyte.

V (L) is the volume of the electrolyte.

N is number of electrons are needed to produce one formate molecule, whose value is two.

F is Faraday's constant whose value (96485 C mol^{-1}).

Q_{Total} (C) is total charge during the experiment

Calculation of energy conversion efficiency

H-cell and flow-cell belong to the half cell and corresponding energy conversion efficiency (EE) was calculated in the cathode. The overpotential of oxygen evolution was assumed to be zero. The EE of formate can be calculated as follow:[1]

$$EE_{half-cell} = \frac{(1.23 + (-E_{foramte})) \times FE_{formate}}{(1.23 + (-E_{applied}))}$$

$E_{formate}$ is the thermodynamic potential (versus RHE) for CRR to formate, which is -0.2 for acetate.

$FE_{formate}$ is the measured faradaic efficiency of formate.

$E_{applied}$ is the applied potential (versus RHE) in three electrode system.

Formate energy efficiency reported in others' work was also calculated in full cell (MEA system):

$$EE_{full-cell} = \frac{(1.23 + (-E_{foramte})) \times FE_{formate}}{-E_{full-cell\ applied}}$$

$EE_{full\text{-}cell\ applied}$ is the full-cell potential applied in the MEA system.

Figures and Tables

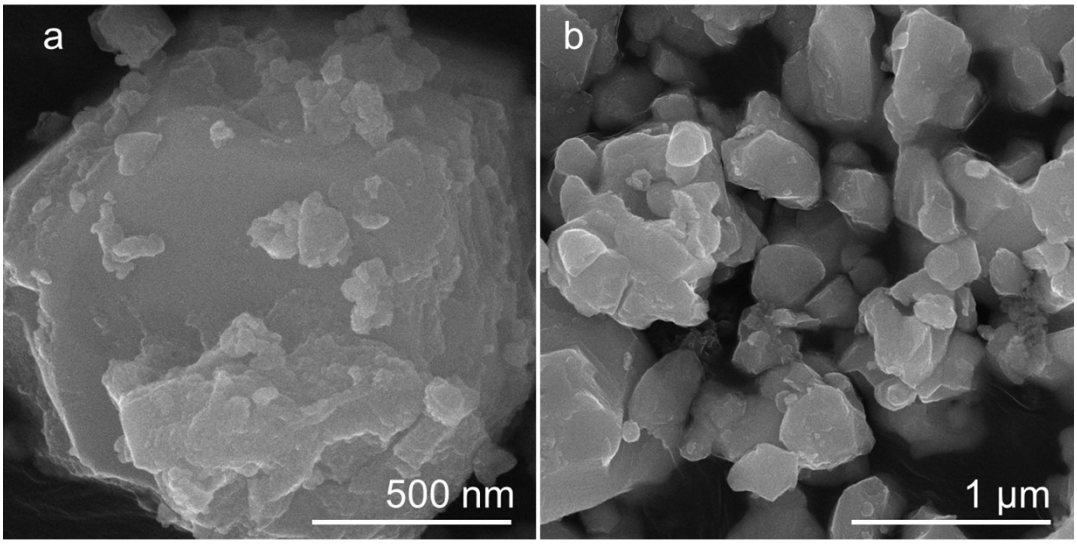

Figure S1 SEM images of (a) $BiOON_4$ and (b) BiO_x.

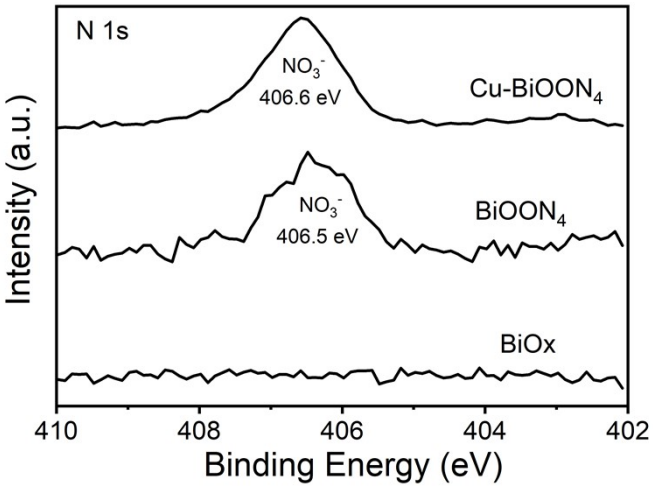

Figure S2 High-resolution XPS of N 1s.

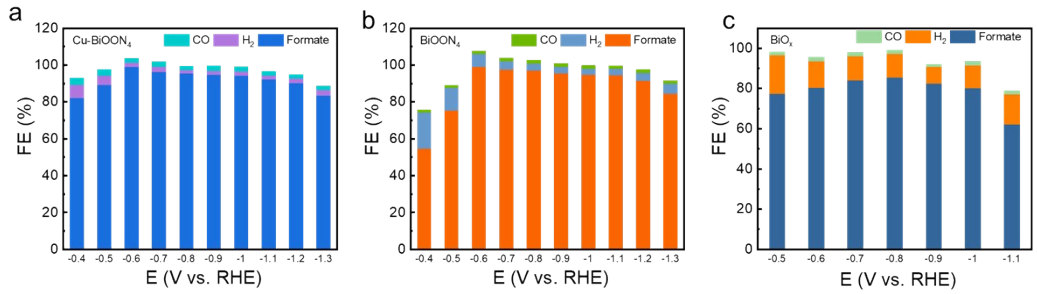

Figure S3 Faradaic efficiencies of products in the H cell.

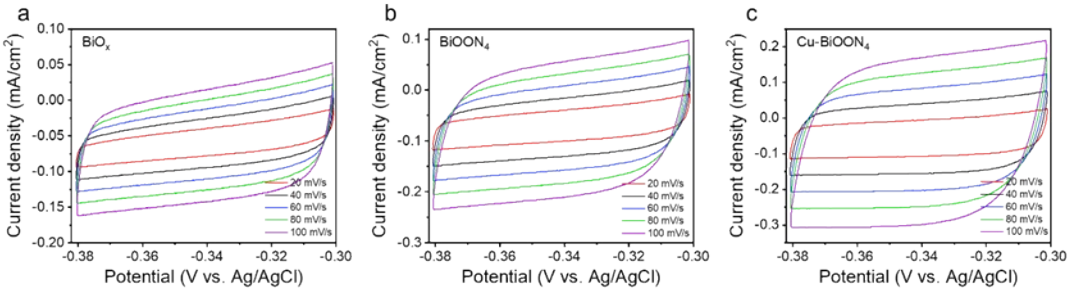

Figure S4 CV curves for (a) BiO_x, (b) $BiOON_4$ and (c) Cu-$BiOON_4$ performed in the region of -0.30 ~ -0.38 V vs. Ag/AgCl at various scan rates in 0.1 M $KHCO_3$ solution.

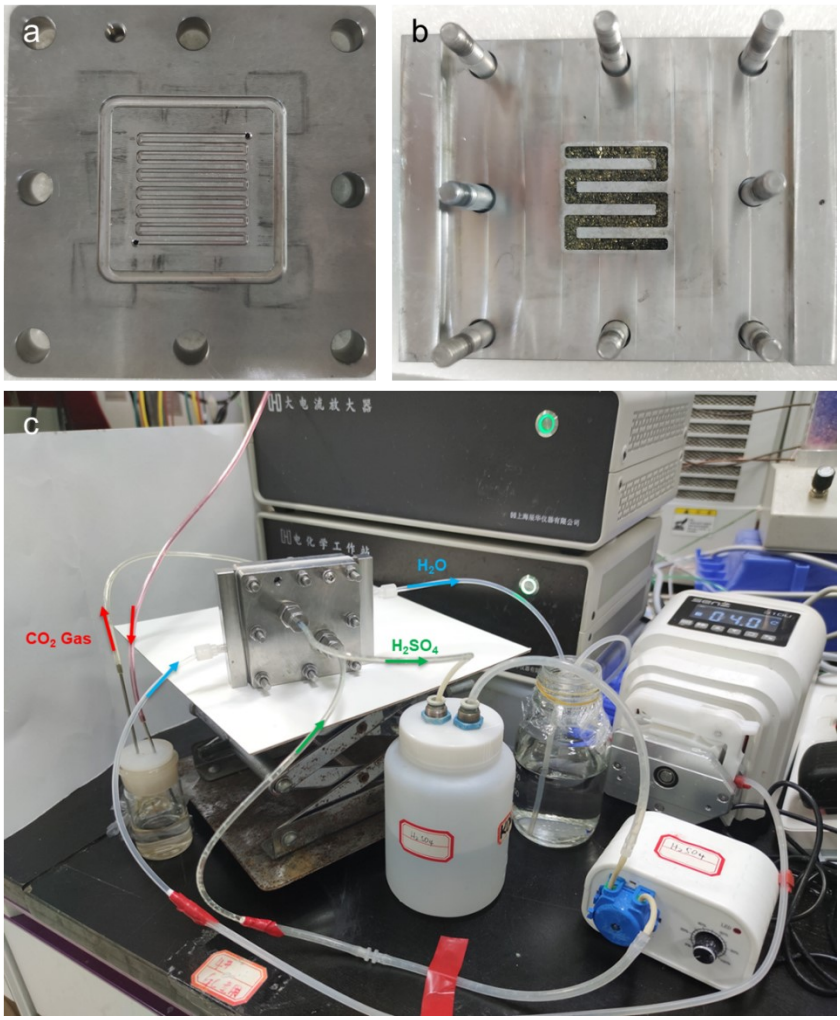

Figure S5 The top view of (a) anode and cathode electrode. (b) The front view of the solid electrolyte layer, which contains a serpentine channel filled with styrene-divinylbenzene copolymer spheres. (c) The diagram of the working device of a solid electrolyte.

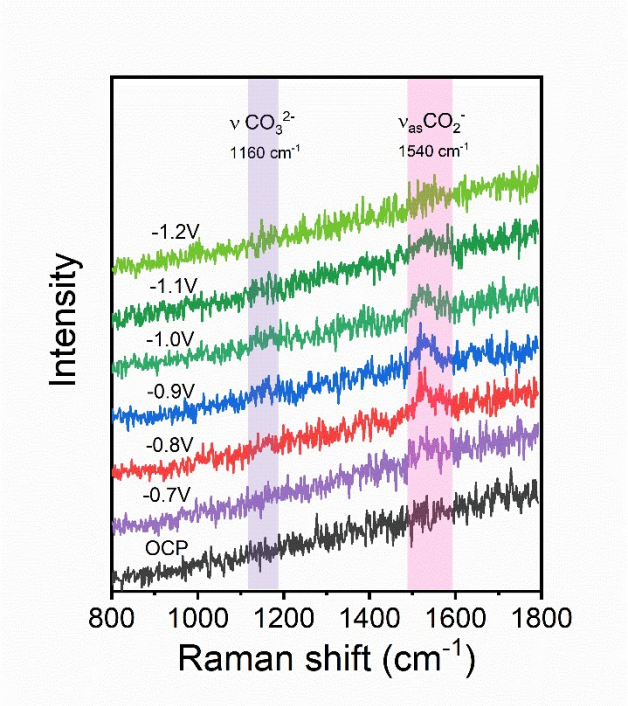

Figure S6 Potential- dependent in situ Raman spectra in 0.1 M $KHCO_3$ electrolyte for $BiOON_4$.

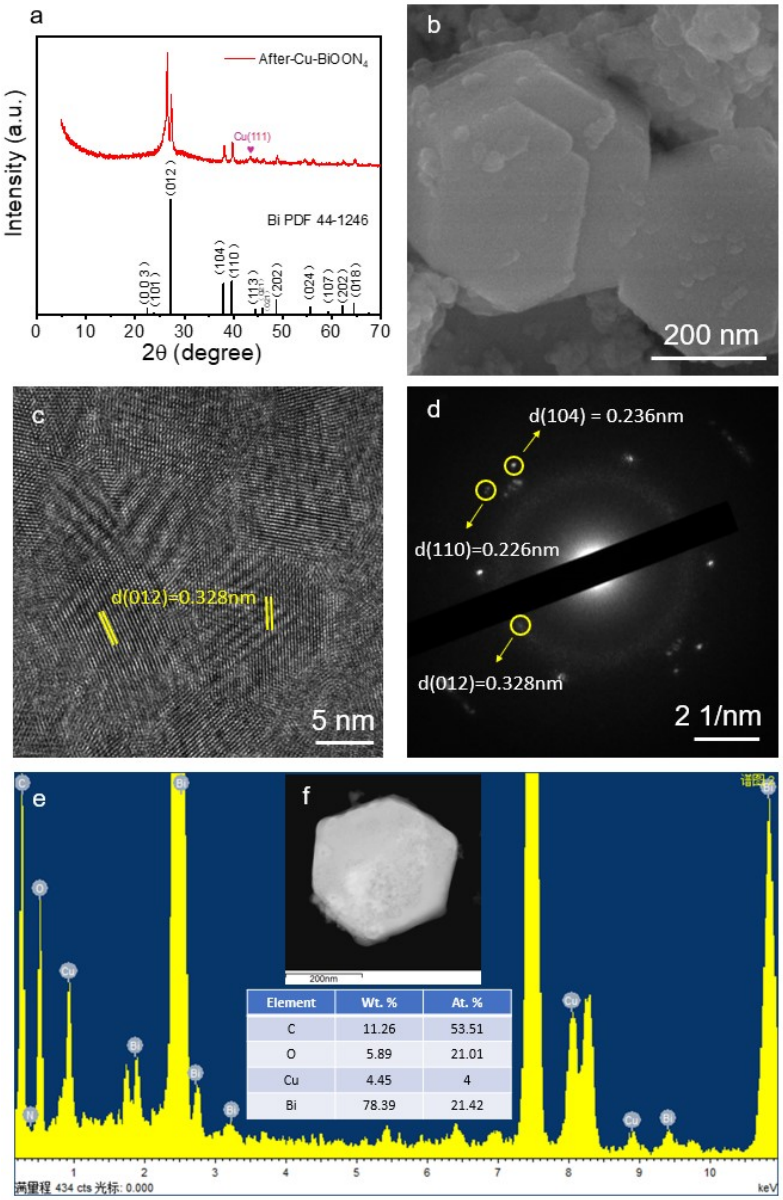

Figure S7 (a) XRD pattern of Cu-$BiOON_4$ after 30 min reduction in CRR, noted as After-Cu-$BiOON_4$. (b) SEM image, (c) high-resolution TEM image and (d) SAED pattern of After-Cu-$BiOON_4$. (f) High-angle annular dark field STEM image of After-Cu-$BiOON_4$ hexagonal nanosheet and (e) corresponding EDS element analysis graph. C and O both came from absorbed HCO_3^- species in $KHCO_3$ electrolyte.

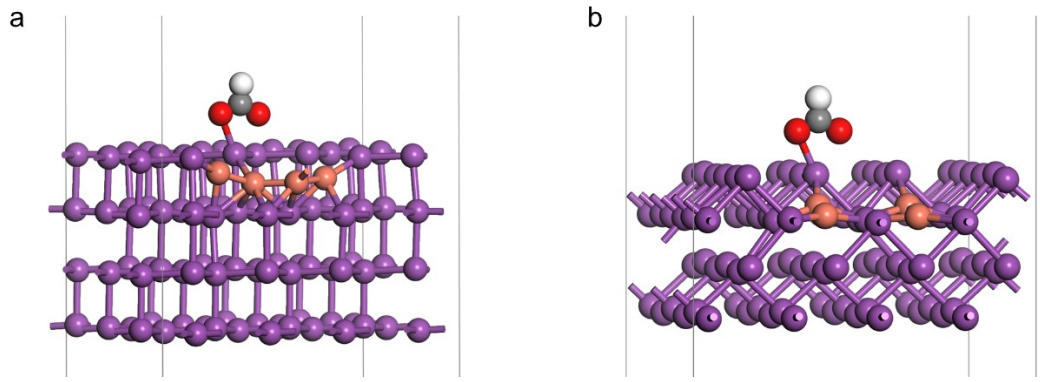

Figure S8 The optimized adsorption models of *OCHO intermediate on (a) 4Cu-Bi(012) and (b) 4Cu-Bi(104).

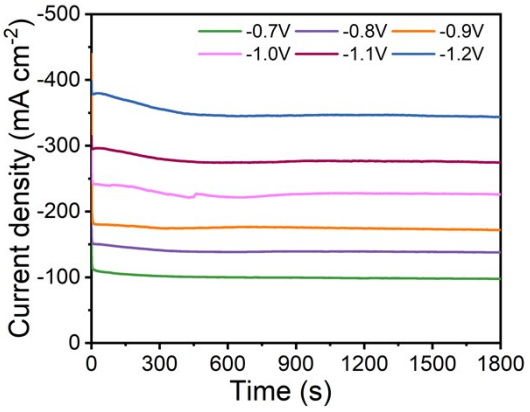

Figure S9 Chronoamperometric responses at different potentials with 1 M KOH electrolytes in the flow cell.

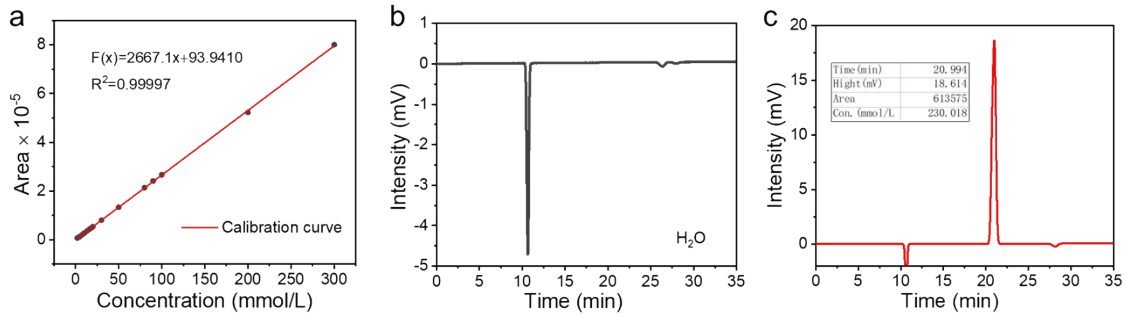

Figure S10 (a) Calibration cure between HCOOH concentration and relative peak area vs H_2O using in the high-performance liquid chromatography (HPLC). The linear correlation coefficient is 0.99997. (b) The original chromatographic column curve of H_2O sample. (c) The curve of catholyte detected by the inspection detector on HPLC was collected from the stability test of Cu-$BiOON_4$ at 2.35 V for 4h in the solid electrolyte device.

Table S1 Elemental content of samples obtained from XPS.

Electrocatalyst	N (at. %)	O (at. %)	Bi (at. %)	Cu (at. %)
Cu-$BiOON_4$	10.0	67.5	19.1	3.4
$BiOON_4$	5.5	69.6	24.9	--
BiO_x	--	68.7	31.3	--

Table S2 Comparison of formate production on various Me-Sn bimetallic catalysts under comparable conditions.

Electrocatalyst	Electrolyte(pH)	FE[a](%)	*E*[b]*(V)*	E[d]*(V)*	ref
Bi nanostructure	0.5M $KHCO_3$	92	-0.9	-0.9	2
Bi nanosheets	0.5M $NaHCO_3$	86	-1.1	–	3
Bi dendrites	0.5M $NaHCO_3$	98	-0.82	-0.72 to -0.92	4
Bismuthene NA	0.5M $KHCO_3$	95	-0.88	-0.75 to -0.95	5
Bi_2S_3-Bi_2O_3	0.1M $KHCO_3$	93.8	-1.1	-1.0 to -1.4	6
Bi-Cu	0.5M $KHCO_3$	95.8	-0.9	-0.9 to -1.0	7
$In_{16}Bi_{84}$ NS	0.5M $NaHCO_3$	~100	-0.94	-0.84 to -1.54	8
$CuBi_2O_4$	0.5M $NaHCO_3$	95	-0.93	-0.83 to -1.03	9
Bi_2CO_3 NS	0.1M $KHCO_3$	92	-1.2	-1.1 to -1.2	10
$CuBi_{75}$	0.5M $KHCO_3$	~100	-0.77	-0.57 to -1.47	11
Cu_1Sn_1	0.5M $NaHCO_3$	95.4	-1.2	-1.2 to -1.3	12
BiCu/CF-0.1	0.5 M $KHCO_3$	94.2	-0.8	-0.7 to -1.1	13
Bi−Cu (2:1)	0.1M $KHCO_3$	94.1	-1.0	-0.8 to -1.2	14
Cu-$BiOON_4$	0.1M $KHCO_3$	~100	-0.6	-0.5 to -1.2	This work

[a]Maximum FE_{HCOOH} under the reported conditions. [b]Overpotential at which the maximum FE is achieved. [c]Current density achieved at the listed overpotential. [d]The potential window of faradaic efficiency (>90%) toward formate.

Table S3 Summary of Sn-based electrocatalyst performance for the reduction of CO_2

Electrocatalyst	Electrolyte	FE[a](%)	E^b(V)	$\|j\|^c$(mA cm^{-2})	EE(%)	ref
Ultra-small SnO_2 nanoparticles	1M $KHCO_3$	64	-1.21	145	27.0	15
	1M KOH	46	-0.9	147	22.2	
Sn	$KHCO_3$ and KOH mixed solution	90	-1.57	200	33.1	16
Bi_2S_3-Bi_2O_3	1M KOH	95.3	-1.0	145	61.1	6
Bi dendrites	0.5M $KHCO_3$	92	-0.82	95	64.2	4
Bi/Bi(Sn)O_x NWs	1M KOH	~100	-0.7	100	74.1	17
		85	-1.0	301	54.5	
Bi_2O_3@C/HB	1M KOH	94	-1.5	285	49.2	18
Bi_2O_3 NTs	1M KOH	98	-0.58	205.8	77.4	19
Cu-$BiOON_4$	1M KOH	96.0	-1.0	220	61.7	This work

to formate in flow cell.

[a]Maximum FE_{HCOOH} under the reported conditions. [b]Potential at which the maximum FE is achieved. [c]Partial current density of formate achieved at the listed overpotential.

Table S4 Summary of the electrocatalyst performance for producing HCOOH in solid electrolyte devices.

Catalyst	Area cm^2	SEE diameter (μm)	E (V)	FE (%)	|J| (mA cm^{-2})	Yield/Time	Anode electrolyte	ref.
2D-Bi	4	300	3.08	93.1	32.1	0.112 M/100 H	0.1 M KOH	20
		50	~3.0	82.7	200	--	0.1 M KOH	
In_2O_3@C	4	50	3.6	~85	30	0.12 M/3 H	1 M H_2SO_4	21
Cu-$BiOON_4$	2.75	300-1000	2.35	92.6	81	0.19 M/4 H	1 M H_2SO_4	This work
			2.45	88.5	116	--		

Reference

1 W. Ma, S. Xie, T. Liu, Q. Fan, J. Ye, F. Sun, Z. Jiang, Q. Zhang, J. Cheng and Y. Wang, *Nat. Catal.*, 2020, **3**, 478–487.

2 P. Lu, D. Gao, H. He, Q. Wang, Z. Liu, S. Dipazir, M. Yuan, W. Zu and G. Zhang, *Nanoscale*, 2019, **11**, 7805–7812.

3 W. Zhang, Y. Hu, L. Ma, G. Zhu, P. Zhao, X. Xue, R. Chen, S. Yang, J. Ma, J. Liu and Z. Jin, *Nano Energy*, 2018, **53**, 808–816.

4 M. Fan, S. Prabhudev, S. Garbarino, J. Qiao, G. A. Botton, D. A. Harrington, A. C. Tavares and D. Guay, *Appl. Catal. B Environ.*, 2020, **274**, 119031.

5 J. Fan, X. Zhao, X. Mao, J. Xu, N. Han, H. Yang, B. Pan, Y. Li, L. Wang and Y. Li, *Adv. Mater.*, 2021, **33**, 2100910.

6 P. F. Sui, C. Xu, M. N. Zhu, S. Liu, Q. Liu and J. L. Luo, *Small*, 2022, **18**, 2105682.

7 L. Peng, Y. Wang, Y. Wang, N. Xu, W. Lou, P. Liu, D. Cai, H. Huang and J. Qiao, *Appl. Catal. B Environ.*, 2021, **288**, 120003.

8 D. Tan, W. Lee, Y. E. Kim, Y. N. Ko, M. H. Youn, Y. E. Jeon, J. Hong, J. E. Park, J. Seo, S. K. Jeong, Y. Choi, H. Choi, H. Y. Kim and K. T. Park, *ACS Appl. Mater. Interfaces*, 2022, **14**, 28890–28899.

9 L. Jia, H. Yang, J. Deng, J. Chen, Y. Zhou, P. Ding, L. Li, N. Han and Y. Li, *Chin. J. Chem.*, 2019, **37**, 497–500.

10 D. Yao, C. Tang, A. Vasileff, X. Zhi, Y. Jiao and S. Z. Qiao, *Angew. Chem. Int. Ed.*, 2021, **60**, 18178–18184.

11 Z. Yang, H. Wang, X. Fei, W. Wang, Y. Zhao, X. Wang, X. Tan, Q. Zhao, H. Wang, J. Zhu, L. Zhou, H. Ning and M. Wu, *Appl. Catal. B Environ.*, 2021, **298**, 120571.

12 M. Zhang, Z. Zhang, Z. Zhao, H. Huang, D. H. Anjum, D. Wang, J.-h. He and K.-W. Huang, *ACS Catal.*, 2021, **11**, 11103–11108.

13 B. Liu, Y. Xie, X. Wang, C. Gao, Z. Chen, J. Wu, H. Meng, Z. Song, S. Du and Z. Ren, *Appl. Catal. B Environ.*, 2022, **301**, 120781.

14 M. Wang, S. Liu, B. Chen, F. Tian and C. Peng, *ACS Sustain. Chem. Eng.*, 2022, **10**, 5693–5701.

15 C. Liang, B. Kim, S. Yang, Y. Liu, C. Francisco Woellner, Z. Li, R. Vajtai, W. Yang, J. Wu, P. J. A. Kenis and P. M. Ajayan, *J. Mater. Chem. A*, 2018, **6**, 10313–10319.

16 D. Kopljar, A. Inan, P. Vindayer, N. Wagner and E. Klemm, *J. Appl. Electrochem.*, 2014, **44**, 1107–1116.

17 Y. Zhao, X. Liu, Z. Liu, X. Lin, J. Lan, Y. Zhang, Y. R. Lu, M. Peng, T. S. Chan and Y. Tan, *Nano Lett.*, 2021, **21**, 6907–6913.

18 S. Q. Liu, E. Shahini, M. R. Gao, L. Gong, P. F. Sui, T. Tang, H. Zeng and J. L. Luo, *ACS Nano*, 2021, **15**, 17757–17768.

19 Q. Gong, P. Ding, M. Xu, X. Zhu, M. Wang, J. Deng, Q. Ma, N. Han, Y. Zhu, J. Lu, Z. Feng, Y. Li, W. Zhou and Y. Li, *Nat. Commun.*, 2019, **10**, 2807.

20 C. Xia, P. Zhu, Q. Jiang, Y. Pan, W. Liang, E. Stavitski, H. N. Alshareef and H. Wang, *Nat. Energy*, 2019, **4**, 776-785.

21 Z. Wang, Y. Zhou, D. Liu, R. Qi, C. Xia, M. Li, B. You and B. Y. Xia, *Angew. Chem. Int. Ed.*, 2022, **61**, 202200552.